Gas Monitoring for Graphene Medical Diagnosis

Subjects: Biochemical Research Methods

Contributor: Hong Chi

The development of graphene and its derivatives in gas-phase biomarker detection was reviewed in terms of the detection principle and the latest detection methods and applications in several common gases, etc.

graphene gas sensing

1. Nitric Oxide

Nitric oxide (NO) is synthesized by L-arginine through nitric oxide synthase (NOS) in various cells such as neutrophils, red blood cells, endothelial cells, macrophages, and nerve cells. The determination of NO content in exhaled air has been used as a marker for judging the degree of acute respiratory infection and inflammation in respiratory diseases [1]. The presence of NO in exhaled gases can be used for rapid detection of lung infections [2], including new coronary pneumonia [3], asthma [4], allergic rhinitis [5] severe acute respiratory syndrome (SARS) [6], and chronic obstructive pulmonary disease [7]. At the same time, continuous monitoring of NO is also essential for coronary heart disease [8], Alzheimer's disease [9], and mental illness [10]. Jiang et al. reported on a chlorinated graphene FET and its application in monitoring of NO under specified physiological requirements [11].

Deng et al. synthesized an antimony tetroxide (Sb_2O_4) nanoflower/rGO nanocomposite material using a simple and environmentally friendly solvothermal method [12]. As shown in **Figure 1**a, the combination of highly electroactive Sb_2O_4 nanoflowers and rGO with a larger specific surface area shows a synergistic effect on the recognition of NO. It can detect the NO released by living cells in real time, effectively distinguishing normal and tumor cells. In this case, the reactive Sb^{4+} and rGO help to achieve rapid electron transfer and the nanoflower structure provides a three-dimensional high-speed channel for NO, making the distance across which the NO must travel to reach the reaction center very short, and thereby obtaining a high mass transfer rate.

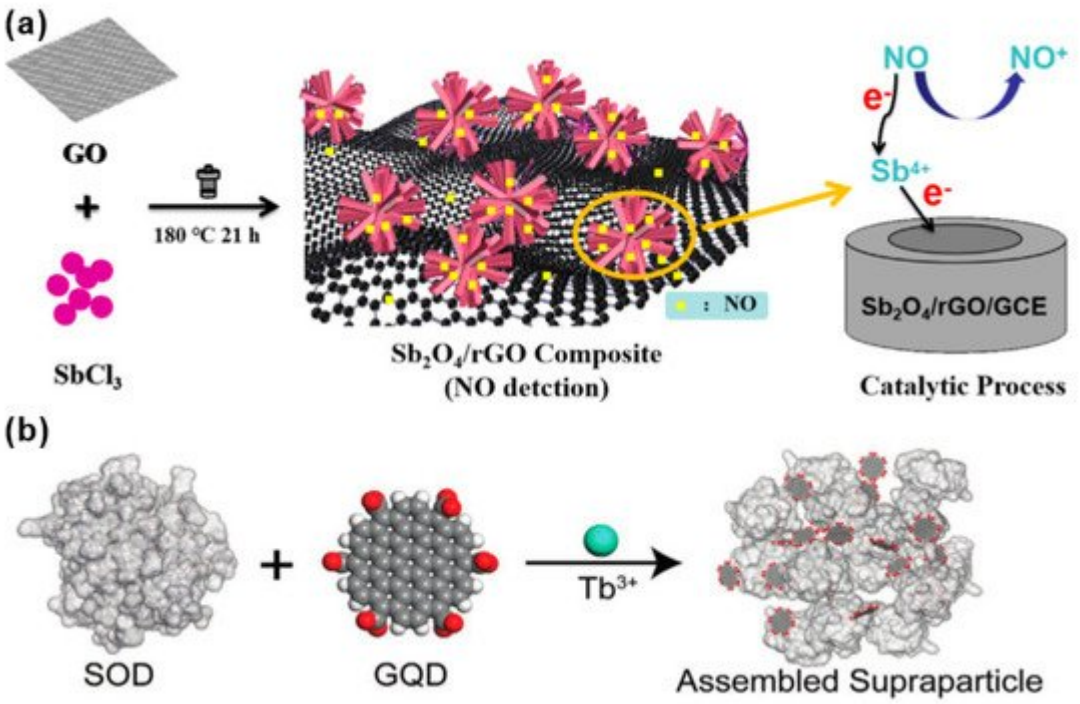

Figure 1. (**a**) Synthetic route of antimony tetroxide (Sb_2O_4) nanoflower/rGO nanocomposite [12]. Copyright (2021), used with permission from Elsevier. (**b**) Schematic diagram of the process of monodisperse superparticles (SPs) prepared by coordinating bridged graphene quantum dots (GQDs) and superoxide dismutase (SOD) using terbium ion as metal [13]. Copyright (2021), used with permission from Wiley.

Inspired by self-limiting nano-components, Qu et al. assembled graphene quantum dots (GQDs) and superoxide dismutase (SOD) into monodisperse superparticles (SPs) [13]. As shown in **Figure 1**b, graphene quantum dots (GQDs) and superoxide dismutase (SOD) were assembled to synthesize GQD–Tb^{3+}–SOD SPs, and were coated on a glass plate for NO sensing test. Superoxide dismutase (SOD) can alternately catalyze the dismutation of superoxide anion free radicals (O^{2-}), usually with copper as the active center. When Cu(II) in SOD is reduced to Cu(I), the fluorescence of the optically active component Tb^{3+} fluorophore is enhanced, which is tightly sandwiched by protein and GQD. Tb^{3+} combines graphene quantum dots (GQDs) and SOD to realize effective energy transfer, thereby “turning on” detection of NO, and realizing reliable monitoring as low as 600 molecules/mL. It is verified that the sensor can achieve ultra-sensitive detection of NO with a concentration as low as 10×10^{-12} M. The sensor opens up a new direction in using self-limiting nano-components. The high sensitivity and non-invasiveness of SP detection means it is widely used in home health monitoring.

Xu et al. constructed an ultra-sensitive NO gas sensor by long-period fiber grating (LFPG) which was covered with GO on a long-period fiber grating (LFPG) that had good sensitivity by refractive index (SRI) changes [14]. The GO was coated on the long-period fiber grating (LPFG) (**Figure 2**a). It can be seen that NO adsorption on the GO depends on two adsorption processes. NO is oxidized by epoxy groups to generate nitrogen dioxide. These complex processes cause NO to be completely removed from the GO surface. The sensor can identify 0–400 ppm NO with high sensitivity. To create more active centers, adjust the band gap of the composite material, and effectively improve the catalytic activity, Qiu et al. used metal oxide nanocrystals (ZnO) to dope redox graphene

with nitrogen (N–rGO). These promote the interaction with the attached metal oxides, create more active centers for gas adsorption, and reduce the hydrolysis rate of $Zn(OAc)_2$ by adding different amounts of NH_4OH dropwise to achieve controllable nucleation. In the experiment, the volume of NH_4OH was controlled to be 0.1, 0.3, and 0.5 mL, and the corresponding products were named NGZ–0.1, NGZ–0.3, and NGZ–0.5 to obtain N–rGO/ZnO (NGZ) hybrid material [15]. At low temperatures, the gas-sensitive response of ZnO nanocrystals on the surface of N–rGO to NO is much better than that of ZnO microcrystals aggregated or formed on the surface of N–rGO alone. The resistance of the zinc oxide channel with a heterojunction in Conduction path 1 in **Figure 2**b,c is much larger than that of the N–RGO channel in Conduction path 2 (R1 ≫ R2). Because metal oxide nanoparticles with a smaller particle size have a p–n heterojunction in NGZ–0.3, which has a strong adsorption effect on NO, the sensitivity of NGZ–0.3 to NO is much greater than that of NGZ–0.1 and NGZ–0.5. **Table 2** summarizes the progress of NO-sensing materials, detection limits, and response/recovery time in recent years.

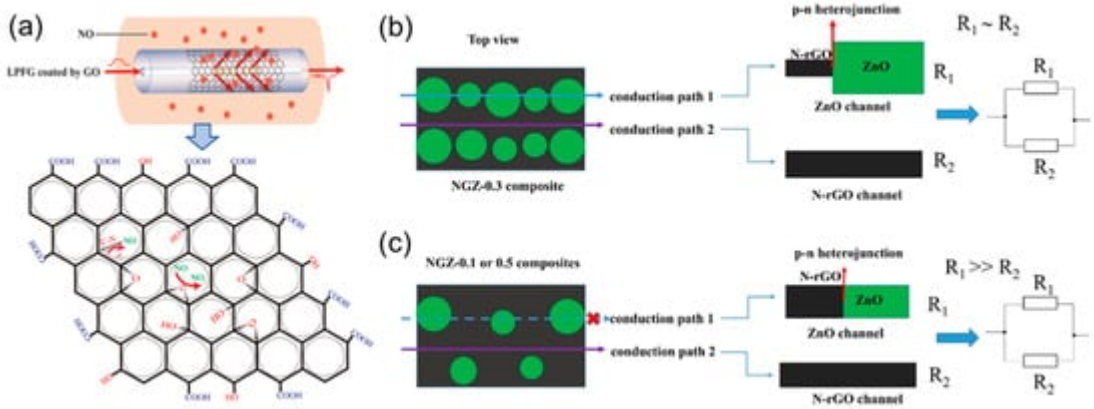

Figure 2. (**a**) The structure of GO–LPFG and the response mechanism to NO [14]. Copyright (2019), used with permission from Elsevier. (**b**) Physical model of NGZ–0.3 (the volume of NH_4OH is 0.3 mL) composite material N–rGO/ZnO (NGZ); (**c**) physical model of NGZ–0.1 or NGZ–0.5 (NH4OH volume 0.1 and 0.5 mL) composite material [15]. Copyright (2020), used with permission from Elsevier.

Table 1. The detection range and response time of other graphene composite materials to NO, NH3 gas.

Material	Gas	Detection Limit	Response/Restore Time	Reference
Pd–rGO	NO	2–420 ppb	1000 s–1 h	[16]
Sub–graphene–hemin	NO	0.3 nM	47–54 ms	[11]
GQD–Tb^{3+}–SOD	NO	600 molecules/mL	500 s	[13]
LPFG coated with GO	NO	0–400 ppm	23.6 min/N.A.	[14]
N–rGO/ZnO	NO	100 ppb	522/303 s	[15]

Material	Gas	Detection Limit	Response/Restore Time	Reference
		300 ppb	478/410 s	
		800 ppb	284/473 s	
Graphene/PS brush	NH_3	≥4.88 ppb	150 s/N.A.	[17]
PPy	NH_3	7.6 ppm	105/182 s	[18]
PPy/GO	NH_3	0.90 ppm	81/116 s	
PPy/rGO	NH_3	0.035 ppm	72/151 s	
PPy/srGO	NH_3	0.00020 ppm	48/234 s	
PPy–rGO	NH_3	10 ppm	~100 s	[19]
PPy/SnO_2/GNR	NH_3	≥0.6 ppm	~100 s/200 s	[20]
MoO_x/GFET	NH_3	≥310 ppb	356 s	[21]
PUF–PPy–GO	NH_3	1.1–182 ppm	~7/13 s	[22]
GO–PANI	NH_3	1 ppm	~5/10 min	[23]

N.A.: not available.

2. Nitrogen Hydride

The production of NH_3 in the human body is related to protein metabolism. Proteins are degraded into non-storable amino acids to be used or metabolized, which leads to the formation of NH_3 [24][25]. Ammonia (NH_3) itself is a toxic and irritating gas. Its accumulation in the human body promotes acidosis in the blood, causes enzyme denaturation, and ultimately leads to death. When the concentration of exhaled ammonia exceeds 2935 ppb, it means that the kidney urea cycle is out of balance. Due to the gas exchange between blood, alveoli, and air, a small amount of ammonia is exhaled in the breath. The main mechanism of ammonia metabolism is the excretion of the urine after the detoxification process, which is the renal urea cycle. In this process, NH_3 is converted into the less toxic soluble compound urea [26]. If the kidneys cannot filter the urea in the blood, urea will enter the body's gas circulation with the blood, and the NH_3 concentration in the breath will increase [26][27][28]. This is why patients with chronic kidney disease (CKD) exhale ammonia gas.

Compared with G, oxygen-containing groups on the surface of GO can enhance the gas sensitivity by interacting with polar gas molecules. There are still some oxygen-containing functional groups on the surface of rGO. To distinguish the influence of polar water molecules on NH_3 detection, Kim et al. studied the response of graphene

gas sensors under two different humidity (RH%) conditions [17]. A passivation layer of polystyrene (PS) brush was used on the surface of silicon dioxide to cover the hydroxyl groups in SiO_2/Si.

Figure 3a shows that the improvement in gas sensitivity may be attributed to the π–π stacking and the formation of hydrogen bonds between PPy and rGO, resulting in a larger surface area and fast carrier transport after the two are recombined. Shahmoradi et al. used an in-situ chemical oxidative polymerization method to prepare polypyrrole (PPy) composites with graphene oxide (GO), reduced graphene oxide (rGO), or p-benzenesulfonic acid sulfonated reduced graphene oxide (srGO) [18]. The sensor response process is shown in **Figure 3**b. The effect of the working temperature of different nanocomposite materials at four temperatures (28, 40, 50, and 60 °C) on the sensor's performance was studied. The PPy/srGO sensor showed the highest detection sensitivity, which was 0.20 ppb~12 ppm NH_3. The response principle is attributed to the charge transfer mechanism between NH_3 and the nanocomposite surface. The electron transfer process of NH_3 molecules to the surface of the p-type polypyrrole sensor is depleted, resulting in an increase in resistance. On the other hand, p-type rGO is donated to electrons. When the PPy/srGO sensor is exposed to NH_3 gas, a hydrogen bond interaction was generated between NH_3 and bare PPy and also between NH_3 and srGO; thereby the electrical resistance was increased. Hsieh et al. further improved the hybrid system of PPy and graphene. They prepared a polypyrrole (PPy)/tin oxide (SnO_2)/graphene nanoribbon (GNR) ternary nanocomposite by using an in-situ chemical oxidation polymerization method [20]. The results showed that the response sensitivity of the PPy/SnO_2/GNR sensor containing 3 wt% SnO_2 nanoparticles in 1 ppm NH_3 is about three times that of pure PPy. **Figure 6**c shows that the PPy-coated SnO_2 and GNR can form covalent bonds. The larger specific surface area contributed by SnO_2 and GNR could further enhance the contact site with PPy and provide many adsorption sites for NH_3 gas. The band gaps of PPy and SnO_2 are 2.81 eV and 3.709 eV, respectively. Thus, the p–n heterojunction formed between p-type PPy and n-type SnO_2 benefits the formation of a self-established depletion layer electric field at the PPy/SnO_2 heterojunction.

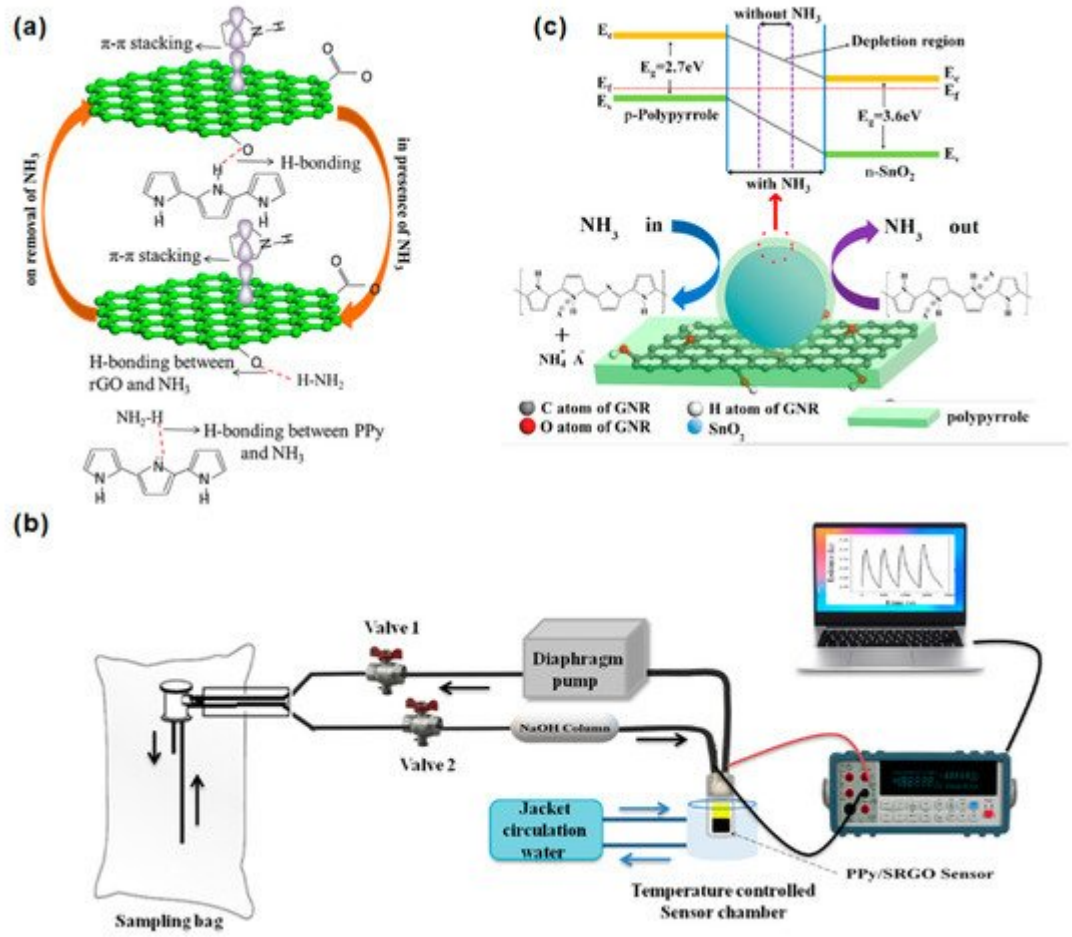

Figure 3. (**a**) Schematic diagram of the interaction between NH_3 and PPy/rGO [19]. Copyright (2017), used with permission from Elsevier. (**b**) Device of PPy/srGO nanocomposite gas sensor [18]. Copyright (2021), used with permission from Elsevier. (**c**) The energy band diagram and sensing mechanism of the PPy/SnO_2/GNR nanocomposite sensor [20]. Copyright (2021), used with permission from Elsevier.

The excellent sensing and recovery performance of the MoO_x/GFET sensor is mainly attributed to the effective adjustment of the height of the Schottky barrier. The energy band in **Figure 4**a indicates the changes in hole density and Fermi energy caused by NH_3 exposure. Under the bias voltage from −50 V to +75 V, the positive change in the back-gate voltage (V_{GS}) causes the Fermi energy valence band to move upward to make it closer to the energy level of NH_3, resulting in a smaller energy difference and less charge transfer between NH_3 and p-type GFET sensors.

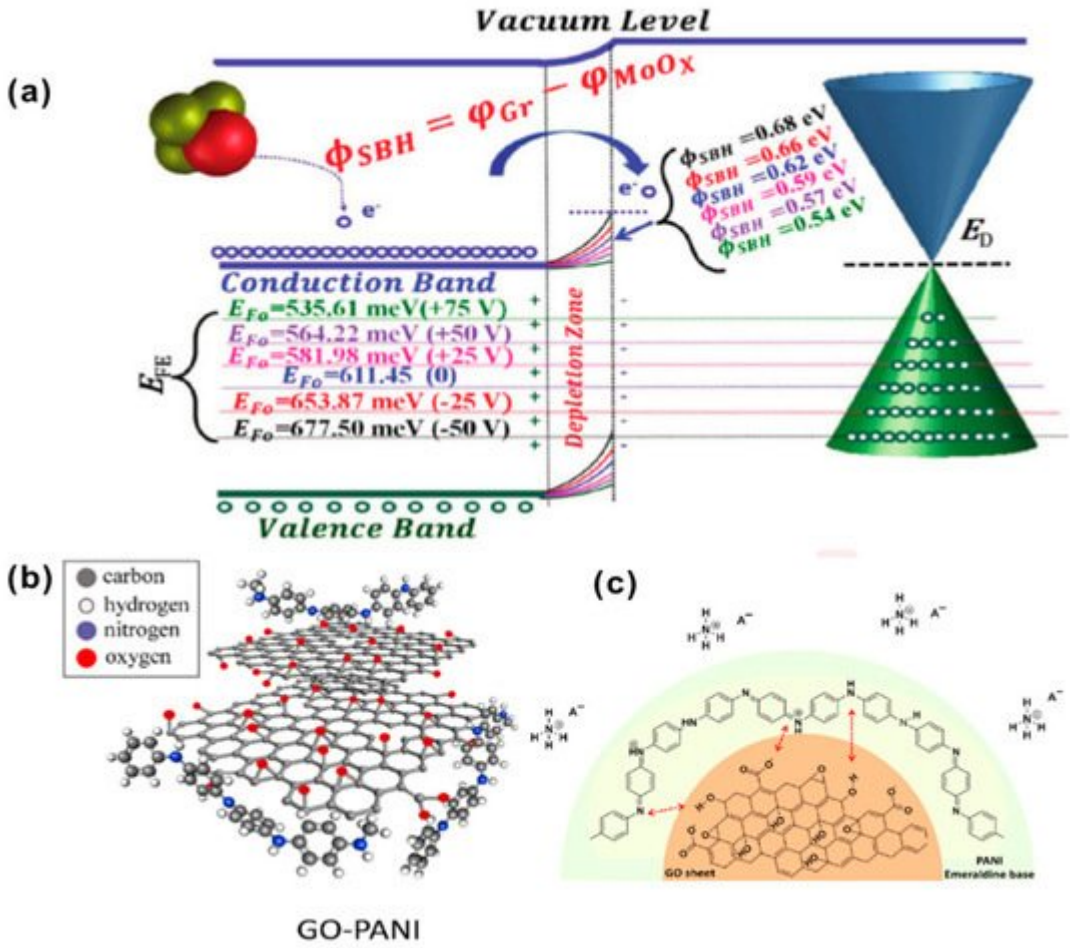

Figure 4. (**a**) Fermi-level tuning diagram in MoOx/graphene composite field-effect transistor sensor (D100) (back gate voltage V_{GS} from −50 to +75 V, electron transfer from NH3 to p-type graphene) [21]. Copyright (2020), used with permission from Elsevier. (**b**) The expanded coil when PANI nanocomposites were pinned to the GO sheets; (**c**) the adsorption mechanism of GO–PANI in ammonia [23]. Copyright (2021), used with permission from Elsevier.

Javadian-Sara et al. explored a microwave-based open-loop resonator (SRR) sensor based on the nanocomposite prepared by the in-situ polymerization of polyaniline (PANI) on the surface of GO [23], as shown in **Figure 4**b. At room temperature, it has a high sensitivity of 0.038 dB ppm^{-1} to low concentration (1–25 ppm) ammonia, a response/recovery time of 150/400 s, and a sensitivity of 0.0045 dB ppm^{-1} to high concentrations (>25 ppm). As shown in **Figure 4**c, when the GO(10%)–PANI nanocomposite is exposed to ammonia gas, due to the acid-base interaction between PANI and ammonia gas, the PANI changes from a conductive form to a non-conductive state. Ammonia gas acts as a base to reduce the aniline ion $R–NH^+$ carriers of PANI through deprotonation, showing a strong de-doping effect and enhancing the internal resistance of PANI. The prepared sensor can selectively detect ammonia in the atmosphere of other higher concentrations of dangerous gases and across a wider range of RH% (15–90%). The response signal can be repeated after 30 days with less than 0.32% variation.

The high efficiency of graphene-based sensor components can be achieved by designing and optimizing their preparation processes, but graphene-based sensors for the physiological analysis of ammonia in breath are still being studied.

3. Sulfide Gas

The cause of bad breath is multifactorial, involving various body organs (mouth, lungs, and stomach). About 90% of all types of bad breath can be classified as intraoral bad breath, which stems from oral-related pathological conditions (dental periodontitis and gingivitis) and physiological characteristics, especially the microbial coating on the tongue [29][30]. The microorganisms in the tongue coating produce a variety of metabolites, including volatile sulfides (VSCs), such as methyl mercaptan (CH_3SH), hydrogen sulfide (H_2S), and dimethyl sulfide (CH_3SCH_3) [31][32][33].

As shown in **Figure 5**a, the adsorption of oxygen causes electrons in the conduction band of the SnO_2 QW to be deprived, causing the energy band to bend and increasing the resistance. The H_2S gas can react with the oxygen adsorbed on the surface, and it is oxidized to sulfur dioxide, making the electrons return to the SnO_2 QW. In this case, it helps to adjust the surface state of the band structure, so that SnO_2 QWs generate more oxygen adsorption sites. At the same time, GO acts as an electron migration channel, which improves the sensitivity of selection. Shewale et al. used a simple air-jet deposition method to uniformly modify GO on copper-doped zinc oxide (CZO) nanostructured films [34]. As shown in **Figure 5**b, the 3CZO/rGO sensor doped with ZnO/rGO (mass fraction of 3 wt% copper nitrate aqueous solution) is fixed on the ceramic microheater with thermal paste. To accurately measure the temperature of the gas sensor, a highly sensitive temperature sensor is installed on the surface of the microheater. The synthesized 3CZO/rGO nanocomposite sensor shows better gas sensitivity to H_2S at room temperature (24 °C) than undoped ZnO/rGO, and a better response to H_2S. The response and recovery time to 100 ppm H_2S are, respectively, 14 s and 32 s, which dramatically improves the potential application of nanocomposite sensors in medical diagnosis. The recent applications of other graphene and its derivatives in the detection of H2S gas biomarkers were summarized in **Table 2**.

Table 3. The detection range and response/recovery time of graphene composites to H_2S gas.

Material	Gas	Detection Limit	Response/Recover Time (s)	References
SnO_2@GO	H_2S	200 ppb	9/23 (54%RH)	[35]
	H_2S		6/21 (93.6%RH)	
ZnO/rGO	H_2S	136 ppb	14/32	[34]
rGO/GaN	H_2S	100 ppm	~800	[36]
(rGO) –NiO(NiOBNG)	H_2S	1 ppm	31/49	[37]
	H_2S	20 ppm	38/44	
	H_2S	50 ppm	28/75	
β–Ga_2O_3/rGO	H_2S	3 ppm	N.A.	[38]
WO_3/rGO	H_2S	32.7 ppb	340/180	[39]

Material	Gas	Detection Limit	Response/Recover Time (s)	References
GQD–SnO_2 QNP/ZnO	H_2S	0.1 ppm	14/13	[40]

N.A.: not available.

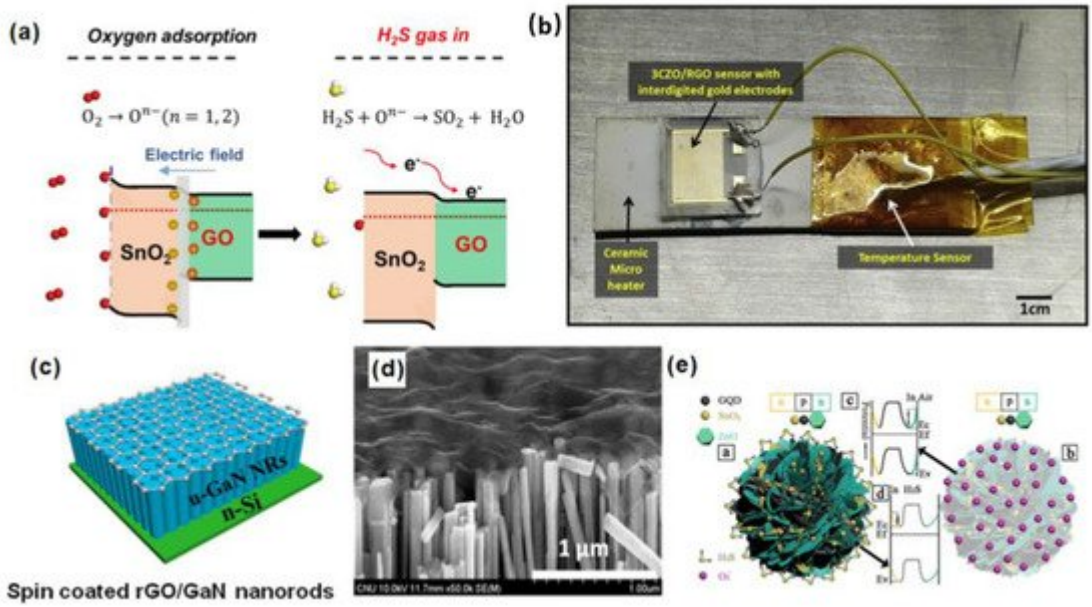

Figure 5. (**a**) Schematic diagram of H_2S adsorption mechanism based on SnO_2@GO gas sensor [35]. Copyright (2020), used with permission from Elsevier. (**b**) CZO/rGO sensor structure [34]. Copyright (2020), used with permission from Elsevier. (**c**) Schematic diagram of rGO)/GaN nanorods (NRS); (**d**) scanning electron microscope (SEM) image of rGO/GaN nanorod (NRS) composite material [36]. Copyright (2020), used with permission from Wiley. (**e**) Schematic diagram of band configuration at the interface of the GQD–SnO_2/ZnO [40]. Copyright (2021), used with permission from the American Chemical Society.

Reddeppa et al. reported a rGO/GaN nanorod (NRs) hybrid system for hydrogen (H_2) and hydrogen sulfide (H_2S) gas sensing at room temperature [36]. **Figure 5**c shows the prepared (rGO)/GaN NRs hybrids. As shown in **Figure 5**d, the surface of the GaN nanorods has a wavy structure without the rGO film, and the spin-coated reduced graphene oxide layer does not penetrate between the nanorods. Compared with pure GaN NRs, rGO/GaN NRs have better gas sensitivity.

4. VOCs

Volatile organic compounds (VOCs) can be generated through various biochemical pathways. The detection of VOC biomarkers can be realized by measuring changes in the electrical, optical, chemical, and chromatic properties of sensitive materials that interact with VOC molecules [41]. Probiotics can regulate intestinal problems and maintain the body's intestinal homeostasis. It is possible to diagnose the balance of human probiotics by detecting changes in the concentration of trimethylamine (TMA) in exhalation [42]. Yu et al. reported the real-time monitoring of TMA in respiration based on the 11–mercaptoundecanoic acid (11–MUA)—Au nanoparticles

(AuNPs)/rGO composite material microgravimetric method [43]. The sensor shows that the lower limit of detection is 5 ppm, and the response time is 30 s. Hexanal and 5-methylundecane are biomarkers of multiple sclerosis (such as Alzheimer's disease (AD) and Parkinson's disease (PD)) [44]. Mazzatenta et al. reported the real-time detection of AD fingerprints in exhalation. A significant change in the accumulated VOC fingerprints was detected in the breath of an AD patient [45]. The recent applications of other graphene and its derivatives in the detection of organic volatile gases that can be used as markers for cancer and other diseases were summarized in **Table 3**.

Table 3. The detection range and response/recovery time of graphene composite materials to VOC gases.

Materials	Gas	Detection Limit	Response/Recovery Time (s)	References
Au NPs–rGO	TMA	≥5 ppm	~30	[43]
C_{60}–g–CNT	ethanol	≥400 ppb	~300/400	[46]
	methanol	≥400 ppb	~300/400	
	acetone	≥400 ppb	~300/400	
	chloroform	≥400 ppb	~300/400	
	toluene	≥400 ppb	~300/400	
	cyclohexane	≥400 ppb	~300/400	
C_{60}–g–rGO	ethanol	≥400 ppb	~300/400	[46]
	methanol	≥400 ppb	~300/400	
	acetone	≥400 ppb	~300/400	
	chloroform	≥400 ppb	~300/400	
	toluene	≥400 ppb	~300/400	
	cyclohexane	≥400 ppb	~300/400	
(Parylene C and GO) MS	toluene	100–300 ppm	164/412	[47]
eG	**acetaldehyd**	≥10 ppm	N.A.	[48]
GO thin film	ethanol	>80 ppm	N.A.	
rGO/SnO_2	acetone	0.25–30 ppm	24/30 (5 ppm)	[49]
$Sn_xTi_{1-x}O_2$/GO	toluene	100 ppb	N.A.	[50]
	acetone	200 ppb	N.A.	
Ag/Fe_3O_4/rGO	acetone	35.81–50 ppm	~50/70	[51]

Materials	Gas	Detection Limit	Response/Recovery Time (s)	References
SiNW/rGO	**acetaldehyd**	1 ppm	30/180	[52]
	cyclohexane	1 ppm	30/60~120	

N.A.: not available.

Ghazi et al. developed a GO microfluidic gas sensor by: (1) 3D printing microchannels coated with a 5-µm-thick parylene carbon layer (propylene polymer). Then, the xylene was used to provide a chemically inert barrier layer. (2) The modified microchannel was coated with GO to improve the specific surface area to volume ratio of the micro-features [47]. The performance was improved. The sensing setup of the microfluidic gas sensor is shown in **Figure 6**a. Compared with ordinary gas sensors, its selectivity to toluene, ethanol, methanol, pentanol, propanol, and hexane increased by 64.4% on average (**Figure 6**b).

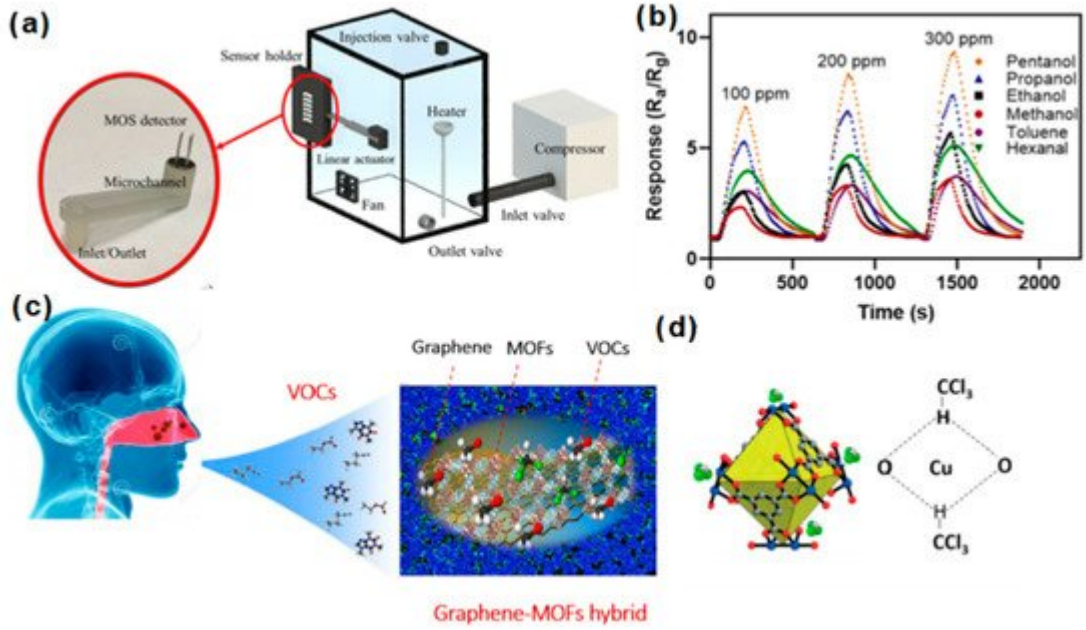

Figure 6. (**a**) Schematic illustration of the microfluidic gas sensor; (**b**) the sensing intensity of the microfluidic gas sensor for different VOCs [47]. Copyright (2022), used with permission from the American Chemical Society. (**c**) Response of graphene and MOF hybrid nanocomposite on exhaled gas; (**d**) the schematic diagram of the hydrogen bond affinity between copper benzene–1,3,5–tricarboxylate (Cu–BTC) and chloroform molecules [53]. Copyright (2020), used with permission from the American Chemical Society.

It is understood that the abnormal concentrations of toluene exhaled by lung cancer patients are in the hundreds of ppb, whereas the normal concentration is about 1–18 ppb. Pargoletti et al. synthesized a $SnxTi_{1-x}O_2$/GO–based material through a simple hydrothermal method, where x is the content ratio of tin [50]. When using 32:1 SnO_2/GO and 32:1 TiO_2/GO, there is excellent selectivity to acetone at a level of 100 ppb. However, when compared with titanium, when a solid solution with a higher tin content (such as 32:1 $Sn_{0.55}Ti_{0.45}O_2$/GO) is used, it shows a higher

performance for the larger non-polar molecule toluene at 350 °C. Tung et al. prepared three different graphene-MOF hybrid nanocomposites, including

Coppere–benzene–1,3,5–tricarboxylate (PG–Cu BTC)), zirconium 1,4–dicarboxybenzene 1,4–dicarboxylate (PG–UIO 66) and 2-methylimidazole zinc salt (PG–ZIF 8). They used this for chemoresistance sensing of VOC biomarkers [53]. As shown in **Figure 6**c, the PG–Cu–BTC sensor was tested against VOC biomarkers, and it showed good selectivity to chloroform. The selectivity principle (**Figure 6**d) is attributed to the hydrogen bond between the chloroform molecule and Cu-BTC.

Diabetes mellitus (DM) is a metabolic disease characterized by high blood sugar caused by insufficient insulin secretion (type I DM), insufficient insulin action (type II DM), or both. Due to hyperglycemia conditions (high blood sugar levels when fasting GI is greater than 7 mmol/L), the excess sugar cannot be metabolized, which induces the decarboxylation of acetoacetate and the dehydrogenation of isopropanol. Large amounts of isopropanol in the liver can produce acetone [54]. The acetone produced in the blood can diffuse through the lungs to the airways, because acetone has a blood/air partition coefficient of 341 at body temperature, and diffuses through urine. Therefore, diabetes can be diagnosed by testing the concentration of acetone in the breath at present [55]. Studies have determined that the average concentration of acetone in the breath of healthy people is 300–900 ppb, and the abnormal concentration of acetone in the breath of diabetes patients exceeds 1800 ppb.

References

1. Willsie, S.K. An Official ATS Clinical Practice Guideline: Interpretation of Exhaled Nitric Oxide Levels (FeNO) for Clinical Applications. Yearb. Pulm. Dis. 2012, 2012, 16.
2. Lassiter, J.B.; Sobhani, H.; Fan, J.A.; Kundu, J.; Capasso, F.; Nordlander, P.; Halas, N.J. Fano resonances in plasmonic nanoclusters: Geometrical and chemical tunability. Nano Lett. 2010, 10, 3184–3189.
3. Exline, M.C.; Stanacevic, M.; Bowman, A.S.; Gouma, P.I. Exhaled nitric oxide detection for diagnosis of COVID-19 in critically ill patients. PLoS ONE 2021, 16, e0257644.
4. Gao, J.; Wu, F. Association between fractional exhaled nitric oxide, sputum induction and peripheral blood eosinophil in uncontrolled asthma. Allergy Asthma Clin. Immunol. 2018, 14, 21.
5. Duong-Quy, S.; Vu-Minh, T.; Hua-Huy, T.; Tang-Thi-Thao, T.; Le-Quang, K.; Tran-Thanh, D.; Doan-Thi-Quynh, N.; Le-Dong, N.N.; Craig, T.J.; Dinh-Xuan, A.T. Study of nasal exhaled nitric oxide levels in diagnosis of allergic rhinitis in subjects with and without asthma. J. Asthma Allergy 2017, 10, 75–82.
6. Keyaerts, E.; Vijgen, L.; Chen, L.; Maes, P.; Hedenstierna, G.; Van Ranst, M. Inhibition of SARS-coronavirus infection in vitro by S-nitroso-N-acetylpenicillamine, a nitric oxide donor compound. Int. J. Infect. Dis. 2004, 8, 223–226.

7. Hu, L.; Gao, S.; Ding, X.; Wang, D.; Jiang, J.; Jin, J.; Jiang, L. Photothermal-Responsive Single-Walled Carbon Nanotube-Based Ultrathin Membranes for On/Off Switchable Separation of Oil-in-Water Nanoemulsions. ACS Nano 2015, 9, 4835–4842.
8. Zhang, P.; Liu, H.; Li, X. Plasmonic CuCo/Carbon Dots: An Unconventional Photocatalyst Used for Photocatalytic Overall Water Splitting. ACS Sustain. Chem. Eng. 2020, 8, 17979–17987.
9. Malinski, T. Nitric Oxide and Nitroxidative Stress in Alzheimer's Disease. J. Alzheimer's Dis. 2007, 11, 207–218.
10. Pitsikas, N. The role of nitric oxide (NO) donors in anxiety. Lights and shadows. Nitric Oxide 2018, 77, 6–11.
11. Jiang, S.; Cheng, R.; Wang, X.; Xue, T.; Liu, Y.; Nel, A.; Huang, Y.; Duan, X. Real-time electrical detection of nitric oxide in biological systems with sub-nanomolar sensitivity. Nat. Commun. 2013, 4, 2225.
12. Deng, X.; Zou, Z.; Zhang, Y.; Gao, J.; Liang, T.; Lu, Z.; Ming Li, C. Synthesis of merit-combined antimony tetroxide nanoflowers/reduced graphene oxide to synergistically boost real-time detection of nitric oxide released from living cells for high sensitivity. J. Colloid Interface Sci. 2021, 581, 465–474.
13. Qu, Z.B.; Zhou, X.; Zhang, M.; Shen, J.; Li, Q.; Xu, F.; Kotov, N.; Fan, C. Metal-Bridged Graphene-Protein Supraparticles for Analog and Digital Nitric Oxide Sensing. Adv. Mater. 2021, 33, e2007900.
14. Xu, B.; Huang, J.; Xu, X.; Zhou, A.; Ding, L. Ultrasensitive NO Gas Sensor Based on the Graphene Oxide-Coated Long-Period Fiber Grating. ACS Appl. Mater. Interfaces 2019, 11, 40868–40874.
15. Qiu, J.; Hu, X.; Min, X.; Quan, W.; Tian, R.; Ji, P.; Zheng, H.; Qin, W.; Wang, H.; Pan, T.; et al. Observation of Switchable Dual-Conductive Channels and Related Nitric Oxide Gas-Sensing Properties in the N-rGO/ZnO Heterogeneous Structure. ACS Appl. Mater. Interfaces 2020, 12, 19755–19767.
16. Li, W.; Geng, X.; Guo, Y.; Rong, J.; Gong, Y.; Wu, L.; Zhang, X.; Li, P.; Xu, J.; Cheng, G.; et al. Reduced Graphene Oxide Electrically Contacted Graphene Sensor for Highly Sensitive Nitric Oxide Detection. ACS Nano 2011, 5, 6955–6961.
17. Kim, S.; Kwak, D.H.; Choi, I.; Hwang, J.; Kwon, B.; Lee, E.; Ye, J.; Lim, H.; Cho, K.; Chung, H.J.; et al. Enhanced Gas Sensing Properties of Graphene Transistor by Reduced Doping with Hydrophobic Polymer Brush as a Surface Modification Layer. ACS Appl. Mater. Interfaces 2020, 12, 55493–55500.
18. Shahmoradi, A.; Hosseini, A.; Akbarinejad, A.; Alizadeh, N. Noninvasive Detection of Ammonia in the Breath of Hemodialysis Patients Using a Highly Sensitive Ammonia Sensor Based on a

Polypyrrole/Sulfonated Graphene Nanocomposite. Anal. Chem. 2021, 93, 6706–6714.

19. Sun, J.; Shu, X.; Tian, Y.; Tong, Z.; Bai, S.; Luo, R.; Li, D.; Liu, C.C. Facile preparation of polypyrrole-reduced graphene oxide hybrid for enhancing NH3 sensing at room temperature. Sens. Actuators B Chem. 2017, 241, 658–664.
20. Hsieh, C.-H.; Xu, L.-H.; Wang, J.-M.; Wu, T.-M. Fabrication of polypyrrole/tin oxide/graphene nanoribbon ternary nanocomposite and its high-performance ammonia gas sensing at room temperature. Mater. Sci. Eng. B 2021, 272, 115317.
21. Falak, A.; Tian, Y.; Yan, L.; Xu, L.; Song, Z.; Hu, H.; Dong, F.; Adamu, B.I.; Zhao, M.; Chen, P.; et al. Ultrathin MoOx/Graphene Hybrid Field Effect Transistor Sensors Prepared Simply by a Shadow Mask Approach for Selective ppb-Level NH3 Sensing with Simultaneous Superior Response and Fast Recovery. Adv. Mater. Interfaces 2020, 7, 1902002.
22. Kim, Y.J.; Kang, H.J.; Moerk, C.T.; Lee, B.-T.; Choi, J.S.; Yim, J.-H. Flexible, biocompatible, and electroconductive Polyurethane foam composites coated with graphene oxide for ammonia detection. Sens. Actuators B Chem. 2021, 344, 130269.
23. Javadian-Saraf, A.; Hosseini, E.; Wiltshire, B.D.; Zarifi, M.H.; Arjmand, M. Graphene oxide/polyaniline-based microwave split-ring resonator: A versatile platform towards ammonia sensing. J. Hazard. Mater. 2021, 418, 126283.
24. Sobhanimatina, M.; Pourmahdian, S.; Tehranchi, M.M. Colorimetric Monitoring of Humidity by Opal Photonic Hydrogel. Polym. Test 2021, 98, 106999.
25. Zhou, J.; Wu, R.; Fu, X.; Wu, J.; Mei, Q. Ratio-Adjustable Upconversion Luminescence Nanoprobe for Ultrasensitive In Vitro Diagnostics. Anal. Chem. 2021, 93, 9299–9303.
26. Oguma, T.; Nagaoka, T.; Kurahashi, M.; Kobayashi, N.; Yamamori, S.; Tsuji, C.; Takiguchi, H.; Niimi, K.; Tomomatsu, H.; Tomomatsu, K.; et al. Clinical contributions of exhaled volatile organic compounds in the diagnosis of lung cancer. PLoS ONE 2017, 12, e0174802.
27. Popa, C.; Petrus, M.; Bratu, A.M. Ammonia and ethylene biomarkers in the respiration of the people with schizophrenia using photoacoustic spectroscopy. J. Biomed. Opt. 2015, 20, 57006.
28. Wojtas, J.; Tittel, F.K.; Stacewicz, T.; Bielecki, Z.; Lewicki, R.; Mikolajczyk, J.; Nowakowski, M.; Szabra, D.; Stefanski, P.; Tarka, J. Cavity-Enhanced Absorption Spectroscopy and Photoacoustic Spectroscopy for Human Breath Analysis. Int. J. Thermophys. 2014, 35, 2215–2225.
29. Seerangaiyan, K.; Juch, F.; Winkel, E.G. Tongue coating: Its characteristics and role in intra-oral halitosis and general health-a review. J. Breath Res. 2018, 12, 034001.
30. Seemann, R.; Conceicao, M.D.; Filippi, A.; Greenman, J.; Lenton, P.; Nachnani, S.; Quirynen, M.; Roldan, S.; Schulze, H.; Sterer, N.; et al. Halitosis management by the general dental practitioner--results of an international consensus workshop. J. Breath Res. 2014, 8, 017101.

31. Yoshida, A.; Yoshimura, M.; Ohara, N.; Yoshimura, S.; Nagashima, S.; Takehara, T.; Nakayama, K. Hydrogen sulfide production from cysteine and homocysteine by periodontal and oral bacteria. J. Periodontol. 2009, 80, 1845–1851.
32. Zhang, L.; Zhou, L.; Xu, N.; Ouyang, Z. A Carbon Dioxide Bubble-Induced Vortex Triggers Co-Assembly of Nanotubes with Controlled Chirality. Angew. Chem. 2017, 129, 8303–8307.
33. Tong, G.; Guan, J.; Zhang, Q. In Situ Generated Gas Bubble-Directed Self-Assembly: Synthesis, and Peculiar Magnetic and Electrochemical Properties of Vertically Aligned Arrays of High-Density Co3O4 Nanotubes. Adv. Funct. Mater. 2013, 23, 2406–2414.
34. Shewale, P.S.; Yun, K.-S. Synthesis and characterization of Cu-doped ZnO/RGO nanocomposites for room-temperature H2S gas sensor. J. Alloys Compd. 2020, 837, 155527.
35. Song, Z.; Yan, J.; Lian, J.; Pu, W.; Jing, L.; Xu, H.; Li, H. Graphene Oxide-Loaded SnO2 Quantum Wires with Sub-4 Nanometer Diameters for Low-Temperature H2S Gas Sensing. ACS Appl. Nano Mater. 2020, 3, 6385–6393.
36. Reddeppa, M.; Park, B.-G.; Kim, M.-D.; Peta, K.R.; Chinh, N.D.; Kim, D.; Kim, S.-G.; Murali, G. H2, H2S gas sensing properties of rGO/GaN nanorods at room temperature: Effect of UV illumination. Sens. Actuators B Chem. 2018, 264, 353–362.
37. Shanmugasundaram, A.; Chinh, N.D.; Jeong, Y.-J.; Hou, T.F.; Kim, D.-S.; Kim, D.; Kim, Y.-B.; Lee, D.-W. Hierarchical nanohybrids of B- and N-codoped graphene/mesoporous NiO nanodisks: An exciting new material for selective sensing of H2S at near ambient temperature. J. Mater. Chem. A 2019, 7, 9263–9278.
38. Balasubramani, V.; Ahamed, A.N.; Chandraleka, S.; Kumar, K.K.; Kuppusamy, M.R.; Sridhar, T.M. Highly Sensitive and Selective H2S Gas Sensor Fabricated with β-Ga2O3/rGO. ECS J. Solid State Sci. Technol. 2020, 9, 055009.
39. Peng, F.; Wang, S.; Yu, W.; Huang, T.; Sun, Y.; Cheng, C.; Chen, X.; Hao, J.; Dai, N. Ultrasensitive ppb-level H2S gas sensor at room temperature based on WO3/rGO hybrids. J. Mater. Sci. Mater. Electron 2020, 31, 5008–5016.
40. Shao, S.; Chen, X.; Chen, Y.; Zhang, L.; Kim, H.W.; Kim, S.S. ZnO Nanosheets Modified with Graphene Quantum Dots and SnO2 Quantum Nanoparticles for Room-Temperature H2S Sensing. ACS Appl. Nano Mater. 2020, 3, 5220–5230.
41. Lord, H.; Yu, Y.; Segal, A.; Pawliszy, J. Breath Analysis and Monitoring by Membrane Extraction with Sorbent Interface. Anal. Chem. 2002, 74, 5650–5657.
42. Grabowska-Polanowska, B.; Faber, J.; Skowron, M.; Miarka, P.; Pietrzycka, A.; Sliwka, I.; Amann, A. Detection of potential chronic kidney disease markers in breath using gas chromatography with mass-spectral detection coupled with thermal desorption method. J. Chromatogr. A 2013, 1301, 179–189.

43. Yu, H.; Xu, P.; Lee, D.W.; Li, X. Porous-layered stack of functionalized AuNP–rGO (gold nanoparticles–reduced graphene oxide) nanosheets as a sensing material for the micro-gravimetric detection of chemical vapor. J. Mater. Chem. A 2013, 1, 4444.
44. Ionescu, R.; Broza, Y.; Shaltieli, H.; Sadeh, D.; Zilberman, Y.; Feng, X.; Glass-Marmor, L.; Lejbkowicz, I.; Mullen, K.; Miller, A.; et al. Detection of multiple sclerosis from exhaled breath using bilayers of polycyclic aromatic hydrocarbons and single-wall carbon nanotubes. ACS Chem. Neurosci. 2011, 2, 687–693.
45. Mazzatenta, A.; Pokorski, M.; Sartucci, F.; Domenici, L.; Di Giulio, C. Volatile organic compounds (VOCs) fingerprint of Alzheimer's disease. Respir. Physiol. Neurobiol. 2015, 209, 81–84.
46. Kim, K.H.; Jahan, S.A.; Kabir, E. A review of breath analysis for diagnosis of human health. TrAC Trends Anal. Chem. 2012, 33, 1–8.
47. Ghazi, M.; Janfaza, S.; Tahmooressi, H.; Tasnim, N.; Hoorfar, M. Selective detection of VOCs using microfluidic gas sensor with embedded cylindrical microfeatures coated with graphene oxide. J. Hazard. Mater. 2021, 424, 127566.
48. Lu, T.; Al-Hamry, A.; Rosolen, J.M.; Hu, Z.; Hao, J.; Wang, Y.; Adiraju, A.; Yu, T.; Matsubara, E.Y.; Kanoun, O. Flexible Impedimetric Electronic Nose for High-Accurate Determination of Individual Volatile Organic Compounds by Tuning the Graphene Sensitive Properties. Chemosensors 2021, 9, 360.
49. Kalidoss, R.; Umapathy, S.; Anandan, R.; Ganesh, V.; Sivalingam, Y. Comparative Study on the Preparation and Gas Sensing Properties of Reduced Graphene Oxide/SnO2 Binary Nanocomposite for Detection of Acetone in Exhaled Breath. Anal. Chem. 2019, 91, 5116–5124.
50. Pargoletti, E.; Verga, S.; Chiarello, G.L.; Longhi, M.; Cerrato, G.; Giordana, A.; Cappelletti, G. Exploring SnxTi1-xO2 Solid Solutions Grown onto Graphene Oxide (GO) as Selective Toluene Gas Sensors. Nanomaterials 2020, 10, 716.
51. Jia, X.; Yu, S.; Cheng, C.; Yang, J.; Li, Y.; Wang, S.; Song, H. Ag nanoparticles modified Fe3O4/reduced graphene oxide and their acetone sensing properties. Mater. Chem. Phys. 2022, 276, 125378.
52. Gautam, V.; Kumar, A.; Kumar, R.; Jain, V.K.; Nagpal, S. Silicon nanowires/reduced graphene oxide nanocomposite based novel sensor platform for detection of cyclohexane and formaldehyde. Mater. Sci. Semicond. Process. 2021, 123, 105571.
53. Tung, T.T.; Tran, M.T.; Feller, J.-F.; Castro, M.; Van Ngo, T.; Hassan, K.; Nine, M.J.; Losic, D. Graphene and metal organic frameworks (MOFs) hybridization for tunable chemoresistive sensors for detection of volatile organic compounds (VOCs) biomarkers. Carbon 2020, 159, 333–344.

54. Jones, A.W. Urine as a Biological Specimen for Forensic Analysis of Alcohol and Variability in the Urine-to-Blood Relationship. Toxicol. Rev. 2006, 25, 15–35.
55. Fan, G.T.; Yang, C.L.; Lin, C.H.; Chen, C.C.; Shih, C.H. Applications of Hadamard transform-gas chromatography/mass spectrometry to the detection of acetone in healthy human and diabetes mellitus patient breath. Talanta 2014, 120, 386–390.